Probing Structural Differences in Prion Protein Isoforms by Tyrosine Nitration†

Christopher W. Lennon,‡,§ Holly D. Cox,§,|| Scott P. Hennelly,‡ Sam J. Chelmo,⊥ and Michele A. McGuirl*,‡

Division of Biological Sciences and the Biomolecular Structure and Dynamics Program, The University of Montana, Missoula, Montana 59812

Received August 22, 2006; Revised Manuscript Received November 29, 2006

ABSTRACT: Two conformational isomers of recombinant hamster prion protein (residues 90−232) have been probed by reaction with two tyrosine nitration reagents, peroxynitrite and tetranitromethane. Two conserved tyrosine residues (tyrosines 149 and 150) are not labeled by either reagent in the normal cellular form of the prion protein. These residues become reactive after the protein has been converted to the β-oligomeric isoform, which is used as a model of the fibrillar form that causes disease. After conversion, a decrease in reactivity is noted for two other conserved residues, tyrosine 225 and tyrosine 226, whereas little to no effect was observed for other tyrosines. Thus, tyrosine nitration has identified two specific regions of the normal prion protein isoform that undergo a change in chemical environment upon conversion to a structure that is enriched in β-sheet.

Prion diseases are a class of fatal neurodegenerative disorders (*1*, *2*) that include Creutzfeldt−Jakob disease, Gerstmann−Sträussler−Scheinker syndrome, kuru and fatal familial insomnia in humans, bovine spongiform encephalopathy (mad cow disease) in cows, chronic wasting in deer and elk, and scrapie in sheep. Prion diseases belong to the larger category of amyloidoses that also includes Alzheimer's, Parkinson's, Huntington's, and amylotrophic lateral sclerosis diseases. The common characteristic of amyloid diseases is the formation of ordered aggregates of misfolded proteins in the brain, which are associated with plaque deposits and neurodegeneration (*3*). Each type of amyloidosis is associated with a specific misfolded protein; prion diseases involve the prion protein (PrP[1]). However, prion diseases are also unique among amyloidoses in that they are transmissible, in addition to being inherited or sporadic (*2*, *4*).

Unlike other infectious agents, prions do not require a nucleic acid component, i.e., DNA or RNA, for infection to occur. Indeed, the name "prion" is derived from the blending of the first two syllables of the term "proteinaceous infectious" particle (*5*). According to the "protein only" hypothesis of prion replication, an infectious, misfolded oligomeric PrP particle causes the normal, noninfectious monomeric cellular form of PrP, called PrP^C, to undergo a conformational change. This conversion event leads to the incorporation of normal PrP monomers into the infectious aggregated particle, ultimately leading to the formation of fibrils. The fibrillar form of PrP is known as PrP^{Sc}, since it was first associated with scrapie. No covalent modifications are known to occur during or after the conversion process; the difference between PrP^C and PrP^{Sc} is purely conformational (*6*, *7*).

Syrian hamster PrP is an extracellular neuronal protein that is made from a 254-amino acid residue precursor protein. Residues 1−22 comprise the signal peptide that is cleaved upon translocation. Residues 233−254 signal for the addition of a glycosylphosphatidylinositol (GPI) lipid anchor at residue 232, which holds PrP in the membrane. These residues are also cleaved during processing. Mature PrP has the ability to form several distinct and stable isoforms. PrP^C is the normal cellular conformation, for which many high-resolution structures from numerous mammalian sources have been determined by both nuclear magnetic resonance (NMR) (*8*−*15*) and X-ray crystallography (*16*−*18*). PrP^C is a soluble monomer dominated by an α-helical C-terminal domain (residues 125−232) and a large unstructured N-terminus (residues 23−89) (*19*). PrP^{Sc} is the pathological conformer that is enriched in β-sheet secondary structure and which forms insoluble fibrils (*20*, *21*).

The insoluble and fibrillar nature of infectious PrP^{Sc} has hampered the elucidation of its structure at the molecular level, in stark contrast with the wealth of data available for PrP^C. However, many gross structural characteristics of PrP^{Sc} have been determined. Treatment with the nonspecific protease proteinase K showed that while PrP^C is sensitive to proteolysis, PrP^{Sc} fibrils can form a resistant core consisting of amino acid residues ∼90−232 (*22*). Mutagenesis studies of the unstructured N-terminal region of PrP

† This work was supported by grants to M.A.M. from the US Army Research (DAMD17- 03-1-0342) and the NIH COBRE program (P20 RR020185-01).

* Corresponding author: Clapp Building 204, Division of Biological Sciences, 32 Campus Drive The University of Montana, Missoula, MT 59812. E-mail: michele.mcguirl@umontana.edu. Tel: (406) 243-4404. Fax: (406) 243-4304.

‡ The University of Montana.

§ Contributed equally to this work.

|| Current address: Department of Pathology, the University of Utah, 50 N. Medical Dr., Salt Lake City, UT 84132.

⊥ Current address: Sanford School of Medicine, the University of South Dakota, 1400 West 22nd St, Sioux Falls, SD 57105.

[1] Abbreviations: AF_4, asymmetric flow field flow fractionation; CD, circular dichroism; ESI, electrospray ionization; GPI, glycosylphosphatidylinositol; MAb, monoclonal antibody; MALDI, matrix assisted laser desorption ionization; MRE, mean residue ellipticity; MS, mass spectrometry; MS/MS tandem mass spectrometry; NMR, nuclear magnetic resonance; PN, peroxynitrite; PrP, prion protein; PrP90, residues 90−232 of hamster prion protein; PrP^C, cellular prion; PrP^{Sc}, scrapie prion; TCA, trichloroacetic acid; TFA, trifluoroacetic acid; TNM, tetranitromethane; TOF, time of flight.

10.1021/bi0617254 CCC: $37.00
Published on Web 03/31/2007

(residues 23−89) indicate that it is not required for infectivity or fibril formation (*23*−*26*), although it does influence these properties (*27*−*29*). Fourier transform infrared (FT-IR) spectroscopy, which measures the frequencies arising from the stretching vibrations of peptide carbonyl groups, has indicated that the transition from PrP^C to PrP^{Sc} is associated with a small loss in α-helicity and a large increase in β-sheet secondary structure (*6*, *30*). The ultrastructure of PrP^{Sc} has also been probed using low-resolution crystallography (*31*, *32*), and several microscopy studies have been conducted with recombinant PrP fibrils (*33*, *34*). Multiple research groups have combined the available biophysical data with computational techniques to generate models for PrP^{Sc} (*31*, *32*, *35*−*39*). Although these models differ significantly in the details of the proposed PrP^{Sc} subunit structures, each includes intersubunit contacts formed by β-strand interactions as the basis for fibril formation. Some molecular details of PrP^{Sc} are also beginning to emerge. Antibody studies have identified selective epitopes in the C-terminal half of PrP that are surface accessible in PrP^{Sc} but not in PrP^C (*40*−*43*). One of these epitopes is a Tyr-Tyr-Arg (YYR) motif, of which there are two in the primary structure (*40*). Cashman and co-workers favor assignment of the second YYR motif (residues 162−164) as the antigenic site (*40*). They also noted changes in tyrosine fluorescence that were consistent with the solvent exposure of at least some Tyr residues upon conversion of PrP^C to the infectious state.

Another PrP isoform that is enriched in β-sheet structure is the β-oligomer. This is a soluble, spherical aggregate (8−12 subunits) produced in vitro at low pH, usually from recombinant PrP^C protein that lacks the GPI anchor (*44*). Recombinant β-oligomer is not infectious, although fibrils of recombinant PrP have been associated with some infectivity (*45*), and the native PrP^{Sc} isoform is clearly pathogenic. The β-oligomer has been suggested to be off the pathway of fibril formation (*46*), but conditions necessary for its formation have been shown to promote their conversion to well-ordered fibrils upon extended incubation (*34*, *46*). While not identical to that of PrP^{Sc}, the FT-IR spectrum of the β-oligomer is also consistent with it having higher β-sheet content (*34*, *44*). This has been confirmed by circular dichroism (CD) spectroscopy, which measures protein secondary structure (*6*, *34*, *44*, *46*). Similar spectroscopic changes are observed when recombinant PrP^C is converted to this β-oligomeric state or to its insoluble fibrillar form, when either full-length PrP (residues 23−232) or the truncated version (residues 90−232, often designated PrP90) is used (*34*, *47*). The similarity in secondary structure, along with the soluble nature of the β-oligomer, makes this isoform an attractive model of the pathogenic fibrillar form. Interestingly, spherical particles composed of 14−28 subunits were made from the physical disruption of infectious PrP^{Sc} fibrils; these were found to be more infectious than the large fibrils, per protein subunit (*48*). However, the relationship between these spherical aggregates and the recombinant β-oligomer is unclear, as structural details are unavailable.

To provide additional molecular details of the differences between PrP^C and the β-enriched state associated with disease, we have undertaken a comparative study of the susceptibilities of PrP^C and the β-oligomer to tyrosine nitration. Since solvent-exposed tyrosyl residues are more susceptible to chemical nitration than buried residues (*49*), we hypothesized that more of the ten Tyr residues present in hamster PrP90 would react with nitrating reagents in the β-oligomeric state, if the β-oligomer is similar to PrP^{Sc}. We tested this by reacting recombinant truncated hamster PrP90 (residues 90−232 containing 10 tyrosyl residues) in its PrP^C and β-oligomer isoforms with two nitrating reagents, peroxynitrite (PN) and tetranitromethane (TNM). Nitration efficiency was then assessed by peptide mapping via mass spectrometry (MS) (*49*, *50*). As anticipated, conformationally dependent labeling patterns were detected. The first YYR motif (residues 149−151) is selectively nitrated in the β-oligomeric state, whereas the two highly solvent-exposed Tyr residues of PrP^C, Y225 and Y226, were less reactive in the β-oligomer.

EXPERIMENTAL PROCEDURES

Production of Recombinant PrP90 Isoforms. The codons for residues 90−232 of Syrian hamster prion protein were subcloned from plasmid pHaPrP (*51*) into $pET24a^+$, creating the expression plasmid pET24PrP90. This construct produces a truncated recombinant protein (PrP90) in which most of the unstructured N-terminal domain has been omitted, along with the C-terminal residues associated with the mammalian GPI anchor. High levels of expression (>15 mg/L) were achieved in *Escherichia coli* BL21(DE3)-Rosetta cells (Novagen, Inc). Typically, 3 L of liquid culture was grown at 37 °C to an OD_{600} of 1.0 in 2xYT (*52*) media supplemented with 50 μg/mL kanamycin and 34 μg/mL chloramphenicol. Expression of PrP90 was then induced with 0.5 mM isopropyl-β-D-thiogalactoside. Cells were harvested 4 h postinduction and frozen overnight.

PrP90 was purified using modifications to a published procedure (*51*). Frozen cells were suspended in lysis buffer (50 mM TrisCl, pH 7.5 containing 100 μg/mL lysozyme and 10 μg/mL DNase I) for 1.5 h at 37 °C with shaking. Inclusion bodies were purified from the lysis pellet by repeated incubation in 50 mM TrisCl, pH 7.5 containing 1% Triton X-100 followed by centrifugation. They were then solubilized in buffer A (0.1 M KPO_4, 8 M urea, pH 8.0) containing protease inhibitor cocktail (Sigma). After centrifugation, the solublized, unfolded protein was batch-bound to 50 mL of Ni(II)-Chelating Sepharose resin (GE Healthcare), which was then poured into a 5 cm diameter column and washed with buffer A until the A_{280} of the eluent dropped below 0.03. PrP90 was refolded on the column by applying a 2 L linear gradient from buffer A to buffer B (0.1 M KPO_4, pH 8.0), followed by washing with several column volumes of buffer B. PrP^C was eluted with buffer B containing 60 mM imidazole. When necessary, further purification was accomplished using hydrophobic interaction chromatography. Briefly, ∼10 mg of PrP90 was loaded onto a HiPrep Phenyl Sepharose 16/10 column (GE Healthcare) in 10 mM KPO_4, 6 M guanidine-HCl, 1 M NH_4SO_4, pH 8, and eluted with a NH_4SO_4 gradient from 1.0 to 0 M in 25 mM TrisCl, pH 8.0 containing 4 M urea. The sample was then extensively dialyzed into 10 mM ammonium acetate buffer, pH 7. The protein was then used for experiments or lyophilized and stored at −20 °C.

To form the β-oligomer, a modification of Baskakov's procedure was used (*53*). The lyophilized PrP^C pellet was first resuspended and unfolded in 10 mM KPO_4, 6 M guanidine-HCl, pH 8 to a final concentration of 120 μM

protein. This was then diluted 6-fold with conversion buffer (60 mM sodium acetate, 160 mM NaCl, 3.6 M urea, pH 3.7) and incubated at 37 °C overnight. Next, the samples were dialyzed into a suitable nitration reaction buffer.

Protein purity and the extent of protease digestion was assessed by SDS/PAGE analysis, performed on a Pharmacia PhastSystem (GE Healthcare) using 8−25% polyacrylamide gels and Coomassie Blue staining, according to the standard protocols suggested by the manufacturer. These include boiling the samples in treatment buffer containing the reductant dithiothreitol and SDS. Bio-Rad Broad Range Molecular Weight Marker was used as a standard. CD spectra were measured on a Jasco 810 spectrophotometer equipped with a Peltier temperature controller. Conversion was also followed by asymmetric flow field flow fractionation (AF_4) on an AF2000 instrument (PostNova, Inc), equipped with in-line UV−vis and 7-angle multiangle light scattering detectors. Samples of 400 pmol or more were injected and focused for 35 s on a polyethersulfone membrane (4 kDa MWCO) with a crossflow of 2 mL/min and a channel flow of 1 mL/min in 25 mM sodium acetate buffer containing 3 M urea, pH 5.0. Peaks were resolved using a 3 mL/min crossflow and a channel flow of 1 mL/min. The concentrations of purified PrP^C samples were determined using the theoretical extinction coefficient (*54*) at 280 nm of 26,025 M^{-1} cm^{-1}. After conversion to the β-oligomer and/or nitration, protein concentration was determined with the Bio-Rad Protein Dye Assay Kit, using untreated PrP^C as the protein standard.

Nitration of PrP Isoforms. All nitration reactions were performed at room temperature, and all experiments were conducted in triplicate. Peroxynitrite (PN) was prepared according to a published procedure (*55*) with the following modification and stored at −70 °C prior to use: a Bio-Logic SFM400 four-syringe quench flow apparatus was used to mix the components, to maximize the yield of potassium peroxynitrite. PN reactions were performed in 200 mM sodium acetate buffer, pH 5.5, containing 10 μM diethylenetriaminepentaacetic acid, whereas 50 mM sodium acetate buffer, pH 5.5 was used for tetranitromethane (TNM) reaction. The protein concentrations in all samples were ∼12 μM. Samples were vortexed during the addition of PN, and the protein−PN mixture was allowed to react for 5 min prior to cleanup. TNM was added to protein under anaerobic conditions, and the reaction was allowed to proceed overnight for PrP^c or 2 h for the β-oligomer.

After nitration, reaction side products were removed by dialysis and the protein was concentrated by precipitation with trichloroacetic acid (TCA). Protein pellets (∼15 μg) were resuspended in 50 mM ammonium bicarbonate buffer, pH 8 containing sequencing-grade trypsin at a ratio of 1:7.5 and digested at 37 °C overnight. Tryptic peptides were reduced in 10 mM dithiothreitol for 1 h at 56 °C, and the solution was dried under vacuum. Peptides were resuspended in 50% acetonitrile and 0.1% trifluoroacetic acid (TFA), mixed 1:1 with α-cyano-4-hydroxycinnamic acid matrix spiked with a 1:5 dilution of Bruker Peptide Calibration Standard I for calibration. Peptide mass spectra were acquired using a MALDI (matrix assisted laser desorption ionization)-TOF (time of flight) mass spectrometer (ABI Voyager DE Pro) at the University of Montana Mass Spectrometry and Proteomics Core Facility. The level of nitration for each tyrosine-containing peptide was estimated by taking the sum of the peak area for each *m*/*z* assigned to the nitrated peptide (+45), the deoxy-nitrated peptide (+29), and the dideoxy-nitrated peptide (+13) and dividing by the total peak area from the modified and unmodified tyrosine-containing peptide. This method accounts for the characteristic loss of one and two oxygens from the nitroTyr group, caused by photodecomposition associated with the UV wavelength of the MALDI laser (*56*). Tyrosine-containing peptides with methionine oxidation, with and without nitration, were also included in the quantitation. The data represent replicates of at least three individual nitrating treatments; replicate MS spectra were collected for at least two digestions of each treatment. Additional potential side-products associated with protein nitration were not encountered. Peptide P1 was detected in separate MALDI experiments using linear mode. For intact protein mass analysis, PrP^c was concentrated by TCA precipitation and the protein pellet was resuspended in 50% acetonitrile, 0.1% TFA at a concentration of 1 μg/μL. The protein was mixed 1:1 with a saturated solution of sinapinic acid matrix and analyzed in linear mode.

The completeness of the protease digestion was assessed in several ways: first, analysis of the MALDI spectra in the high mass range did not show the presence of any native masses corresponding to undigested PrP; most of the signals arose from fragments of <3000 amu. SDS/PAGE showed no bands larger than 5000 Da, which was the lower limit of the gel resolution. Over 90% of the theoretical tryptic peptides were detected, and hard-to-cleave recognition sites (R/K followed by P) were cleaved with high efficiency—in most cases, no missed cleavages were detectable.

It was possible that Tyr nitration might have caused a difference in desorption from the MALDI matrix compared with the un-nitrated peptide, which would lead to errors in quantitation of nitration yields. To assess this possibility, the peak intensities of the non-nitrated Tyr-containing peptides from control samples were analyzed with respect to the intensity of an internal control—a non-Tyr containing PrP peptide (the sum of the peptide containing residues 137−148 and its Met-oxidized form). Similar calculations were done for treated samples, using the sum of the intensities for all forms of each tryptic peptide that were detected by MALDI. (The different forms were identified using MASCOT, after inclusion of the nitro-Tyr mass to the possible modifications list.) Differences in detection efficiency due to *nitration-dependent* desorption would manifest as variations in the summed intensity relative to the internal control. However, this did not occur for any of the peptides, regardless of the efficiency of nitration. Thus, it appears that the nitrated peptides "fly", that is, they desorb from the matrix, as well as their unmodified counterparts. External calibration was also performed using Bruker Peptide Calibration Standards I. Only samples that gave typical signal responses relative to the internal and external controls are reported.

To confirm the site of nitration on tryptic peptides containing more than one tyrosine, sequence information was obtained by electrospray ionization (ESI) tandem mass spectrometry (MS/MS) analysis using a QTOF micro (Waters, Milford, MA). For sequence analysis of the YYR-peptide 149−151, cyanogen bromide digestion was performed on TCA precipitated protein pellets (15 μg) in 70%

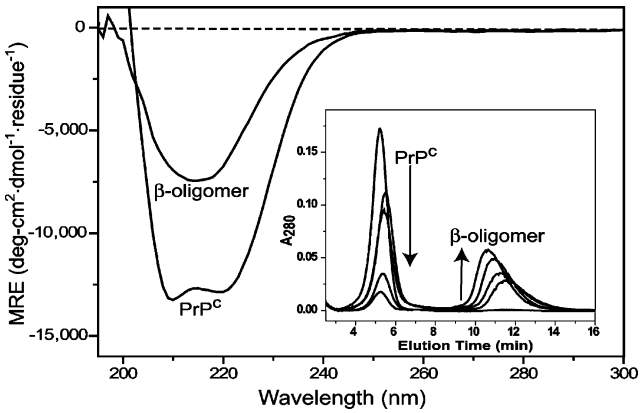

FIGURE 1: CD spectra of PrP conformational isomers. Inset: The AF_4 elution profiles (detection at 280 nm) showing the time course of the chemical conversion of PrP^c to the β-oligomer. Times of conversion: $t = 0$, 15 s, 30 s, 30 min, and 160 min.

TFA at room temperature for 24 h and the digestion solution was removed under vacuum. Peptides from both trypsin and cyanogen bromide digestion were resuspended in 2% acetonitrile, 0.1% formic acid and separated by capillary liquid chromatography using a CapLC XE (Waters) coupled to the ESI source of the QTOF micro. The peptides were concentrated and desalted with an in-line C_{18} PepMap Nano-Precolumn, 5 mm × 300 μm, 5 μm particle size (Dionex) followed by reversed phase separation on a Waters C_{18} capillary column (15 cm × 75 μm i.d., 3 μm particle size). Peptides were eluted from the column with a 70 min linear gradient of acetonitrile from 10 to 40% in 0.1% formic acid. The voltages were set at 3800 V for the capillary, 38 V for the sample cone, and 3.0 V for the extraction cone. Mass spectra were acquired between the range of 200−1500 *m*/*z* followed by data-dependent selection of ions for ms/ms. To enhance the selection of low abundance nitropeptides for MS/MS, only ions with *m*/*z* values that corresponded to nitropeptide masses with a 2+ or 3+ charge state were selected for collision induced dissociation fragmentation. Ions with *m*/*z* values corresponding to the unmodified peptides were not selected for MS/MS. Collision voltages were dependent upon the *m*/*z* and charge state of the parent ion. MS/MS spectra were analyzed using Mascot Daemon (Matrix Science) to search a database containing the hamster PrP90 sequence. Methionine oxidation and nitro-tyrosine were selected as variable modifications. Mass accuracy was set to 50 ppm for peptide tolerance and 0.2 Da for MS/MS tolerance. Replicate MS/MS spectra were acquired on different days and different samples, and the number of times a mononitrated peptide was identified by Mascot was averaged over several runs.

Solvent exposure and secondary structure were determined using MOLMOL software (*57*), using PDB structure 1B10 (*14*). Deconvolution of the CD spectra was performed using the DICHROWEB server (*58*, *59*) and the CDSSTR program, using Reference Set #3 using data collected from 185 to 240 nm. Twenty-five scans were averaged; data collection was performed at 20 °C in a 0.1 or 0.2 mm cuvette on protein samples in the concentration range from 7 to 14 μM.

RESULTS

Protein Purification and Characterization. Using the BL21(DE3)-Rosetta/pET24PrP90 expression system, over 10 mg of PrP^C was routinely obtained per liter of culture, at a purity level of over 95%. The protein is produced as inclusion bodies that are readily purified from the cell paste. Refolding of the protein on the Ni(II)-chelating column leads to the formation of PrP^C, which may be converted to its β-rich conformational isomer. The CD spectra of the PrP^C and β-oligomeric forms of PrP90 are displayed in Figure 1. The high α-helical content of the PrP^C conformer is evident by both the overall shape (two negative peaks at 209 and 222 nm) and the large mean residue ellipticity (MRE) value ($-13{,}000 \pm 1000$ deg-cm^2 dmol^{-1} residue^{-1}) at 222 nm. After conversion, the CD spectrum takes on the characteristics of a β-sheet protein, with a single negative peak centered at 214 nm and a smaller MRE value of -7500 ± 500 deg-cm^2 dmol^{-1} residue^{-1}. Analysis of the two isoforms by asymmetric flow field flow fractionation (AF_4) using in-line UV (Figure 1, inset) and dynamic light scattering detection confirms that PrP^C is a monomeric species and that the β-oligomer is an octamer. This is consistent with published reports that the β-oligomeric form of both PrP90 and the full-length recombinant protein (residues 23−232) contains 8−12 PrP subunits (*46*, *47*, *60*, *61*). Conversion to the β-oligomer is efficient, with only ∼5−10% remaining in the PrP^C state after overnight reaction. This fraction was readily removed from the β-oligomer by AF_4 separation. Reinjection of the purified β-oligomer peak did not show any significant re-formation of PrP^C (data not shown), even after several days of storage, although some PrP^C formation was detectable after several weeks.

Table 1: Deconvolution and Analysis of the CD Spectra of PrP Isoforms Using DICHROWEB

	PrP^C		β-oligomer
secondary structure type	from NMR	from CD	from CD
helix	45%	36%	8%
β-sheet	6%	20%	33%
turn	15%	19%	25%
random coil	34%	25%	34%

The secondary structure determined from the NMR structures (PDB 1B10, (*14*)) by MOLMOL (*57*) agrees relatively well with the value predicted from analysis of the CD spectrum (Table 1). However, the amount of β-sheet is overestimated by the CD deconvolution program. The use of six other reference sets did not improve this result and led to poorer overall fits (data not shown). In spite of this anomaly, the deconvolution analysis clearly show that conversion to the β-oligomer is associated with a substantial decrease in α-helix and an increase in both β-sheet and random coil secondary structures.

MALDI-TOF mass spectrometry of the intact protein indicates that the N-terminal methionine encoded by the vector is processed by the *E. coli* host (theoretical mass with N-terminal Met, 16 462.2 Da; without N-terminal Met, 16 331.1 Da; experimental mass 16 329 ± 2 Da). This N-terminal processing is expected for cytosolic proteins when the side chain of the penultimate amino acid, in this case Gly90 of PrP, is small (*62*). MALDI-TOF analysis of a tryptic digest of the recombinant protein indicates that the disulfide bond between the two existing Cys residues, Cys179 and Cys214, is also intact. This results in the presence of a

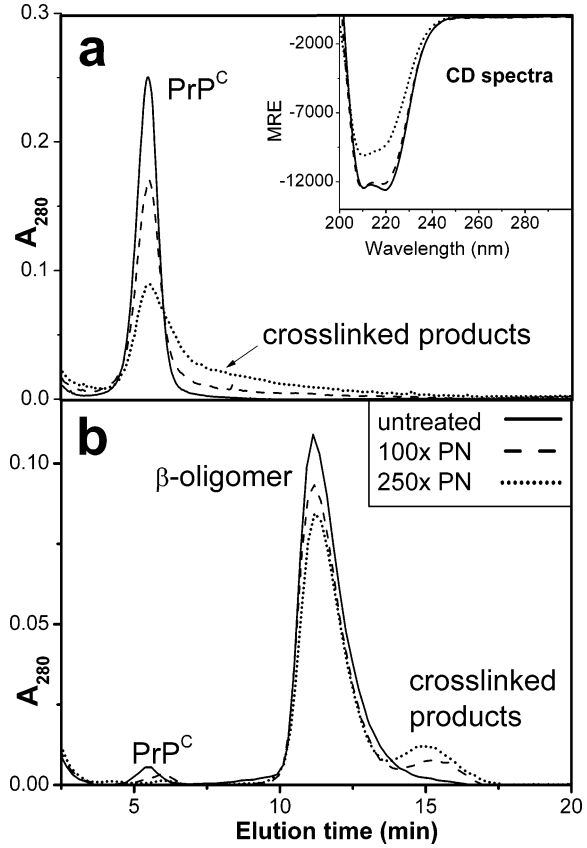

FIGURE 2: AF_4 elution profiles of the PrP isoforms treated with increasing concentrations of PN: (—) untreated control, (- - -) 100× PN reaction, (•••) 250× PN reaction. (a) The PrP^C isoform, with the corresponding CD spectra presented (inset). (b) The β-oligomer.

peak with the average mass of 3732.42 Da detected in linear mode that disappears upon peptide treatment with 10 mM dithiothreitol.

Reaction of PrP90 Isoforms by Peroxynitrite and Tetranitromethane. Initial nitration experiments used a wide range of nitrating reagent concentrations. However, when PrP^C is reacted with PN at concentrations ≥150-fold over protein (15-fold over Tyr residues), AF_4 analysis showed the presence of higher molecular weight species in these samples (Figure 2a). Furthermore, the CD spectra indicate a significant loss in α-helicity at high concentrations of PN (Figure 2a, inset). The higher ordered aggregates persisted even in an SDS/PAGE gel (Figure 3), indicating that the newly formed aggregates represent covalently cross-linked subunits. Similar results were obtained when the β-oligomer was labeled with 250× PN or TNM (Figures 2b and 3). Thus, subsequent experiments were restricted to treatment with 100× nitrating reagents (10-fold excess over Tyr residues) for the β-oligomer and 100× PN for PrP^C, and the structural integrity of each sample was verified after treatment by CD and AF_4 analysis. Under these conditions, PN effectively labeled both PrP^C and the β-oligomer, whereas TNM reacted well with the β-oligomer but poorly with PrP^C (Table 2). Using a higher concentration of TNM (1000×) increased the amount of nitro-Tyr formation in PrP^C to levels comparable to the 100× PN reactions. It is interesting that when PrP^C is treated with 1000× TNM, no evidence of cross-link formation or secondary structure changes was found, as judged by CD, AF_4, and SDS/PAGE techniques.

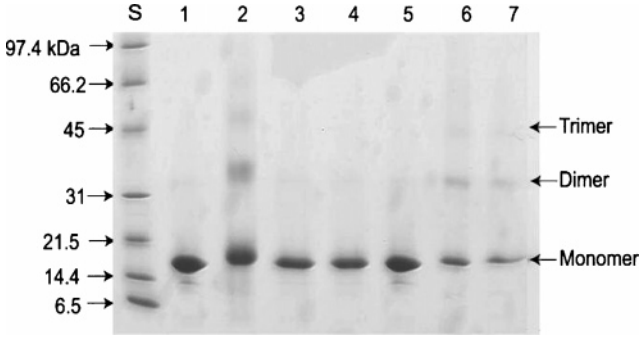

FIGURE 3: SDS/PAGE analysis of PN and TNM reactions with PrP^C and the β-oligomer: lane S, MW standard; lane 1, PrP^c untreated control; lane 2, PrP^c + 250× PN; lane 3, PrP^c + 250× TNM; lane 4; PrP^c + 1000× TNM; lane 5, β-oligomer untreated control; lane 6, β-oligomer + 250× PN; lane 7, β-oligomer + 250× TNM.

Trypsin, which cuts after Lys or Arg residues, produces six Tyr-containing peptides from PrP90 when digestion is followed by disulfide reduction. The tryptic peptide fragments from PrP90 conformers that were treated with either PN or TNM, or from untreated control samples, were analyzed by mass spectrometry. MALDI-TOF MS was used to determine which Tyr residues were labeled and the degree of nitration (Figure 4). Some methionine oxidation was also observed. For peptides containing nitro-Tyr, the expected MALDI-specific fragmentation pattern was observed; the nitro-Tyr peptide (+45) is partially degraded by the MALDI laser to produce fragments with masses corresponding to the loss of one or two oxygens (Figure 4C) (*56*). The signals for these masses were summed to provide the total nitration signal; the results for an average of three nitration reactions are summarized in Table 2. Except for the nitrated P5 peptide, which was difficult to detect by MALDI-TOF, the nitration levels of the Tyr-containing peptides were very consistent across the replicate reactions and digestions. Thus, the estimate of nitration for Y218 is more uncertain than for other Tyr residues.

Patterns of Tyr Nitration in PrP^C. In cases where PN-labeled peptides contained more than one possible site of nitration, tandem mass spectrometry (ESI-MS/MS, Figure 5) was used to determine the site(s) of modification. Since the tryptic peptide containing the first YYR motif (Y149-Y150-R151) is small, aliquots of the nitrated protein were digested with cyanogen bromide to produce a larger peptide spanning residues 140−154 containing this motif (*63*).

Peroxynitrite treatment of PrP^C results in the nitration of six Tyr residues on four tryptic peptides (Table 2). A small amount of nitration was detected at Y128 (peptide P1). No nitration of Y149 or Y150 (peptide P2, part of the first YYR motif) or of Y169 (peptide P4) was observed. Peptide P3, which contains three Tyr residues, was mononitrated at low levels. Multiple tandem MS/MS analyses of the mononitrated P3 peptide showed that, of the three Tyr residues, only Y162 and Y163 (part of the second YYR motif) were susceptible to nitration; no mononitrated product containing nitro-Y157 was ever detected. Nitration at Y162 was detected twice as often as nitration at Y163 (See Figure 5). Y218 (peptide P5) was nitrated at an intermediate level. Peptide P6, which contains Y225 and Y226, was nitrated at the highest levels (70−90%). Nitration at Y226 was favored over Y225 in the

Table 2: MALDI/TOF Analysis of Tyr-Containing PrP Peptides Produced by Trypsin Digestion[a]

tryptic peptide sequence (% SASA)		PrP^C PN 100×	PrP^C TNM 100×	PrP^C TNM 1000×	β-oligomer PN 100×	β-oligomer TNM 100×
P1 (residues 111−136) HMAGAAAAGAVVGGLGG**Y**$_{128}$MLGSAMSR (Y128, 5.6%)		+	−	−	+	−
P2 (residues 149−151) **Y**$_{149}$**Y**$_{150}$R (Y149, 13.7%; Y150, 2.8%)	mononitration dinitration	− −	− −	− −	+++ −	+++ −
P3 (residues 157−164) **Y**$_{157}$PNQV**Y**$_{162}$**Y**$_{163}$R (Y157, 2%; Y162, 11.7%; Y163, 3.3%)	mononitration dinitration trinitration	+ − −	− − −	+ − −	+ − −	++ − −
P4 (residues 165−185) PVDQ**Y**$_{169}$NNQNNFVHDCVNITIK (Y169, 16.4%)		−	−	++	+	+
P5 (residues 209−220) VVEQMCTTQ**Y**$_{218}$QK (Y218, 5.6%)		+++	−	+++	++	++
P6 (residues 221−229) ESQA**Y**$_{225}$**Y**$_{226}$DGR (Y225, 39%; Y226, 59%)	mononitration dinitration	++++ ++	+ −	++++ ++	++ −	++ −

[a] The solvent accessible surface area (SASA) shown is the average value for all NMR solution structures from PDB no. 1B10, using the program MOLMOL. Nitration key: −, 0 to 5% nitration; +, 6 to 20% nitration; ++, 21 to 45% nitration; +++, 46−70% nitration; ++++, 71 to 100% nitration.

mononitrated peptide, but a significant amount of the dinitrated P6 peptide was also detected (see Figure 4C).

The average solvent accessible surface area was calculated using MOLMOL (*57*) for each Tyr residue, from the 25 best NMR solution structures found in PDB Accession No. 1B10 (*14*) (see Figure 6 for one structure). Y226 and Y225 are quite surface exposed and are the most readily nitrated. However, when the solvent accessibility of the Tyr residues is low (as is the case for the other 8 Tyr residues), the degree of nitration does not appear to correlate with surface exposure.

TNM, which nitrates by a different mechanism than PN (*64*), was much less reactive with PrP^C than PN; the only peptide that was found to be nitrated by 100× TNM was P6, which contains Y225 and Y226. When 1000× TNM was used to label PrP^C, higher levels of nitration were achieved. Analysis of the digested samples from 1000× TNM treatment showed that peptides P3 (Y157, Y162, Y163), P5 (Y218), and P6 (Y225, Y226) were labeled to a similar extent as when 100× PN was used. However, the higher concentration of TNM also labeled at P4 (Y169), which was not labeled by PN. Another difference between reagent reactivity was noted in P1 (Y128), which did not label with either concentration of TNM used but which was nitrated at low levels with PN.

As a whole, the data generated from both nitrating reagents show that, in PrP^C, the most solvent exposed tyrosyl residues found in the C-terminal YYD are the most reactive toward nitration. The first YYR motif (Y149-Y150-R151) is unreactive toward both reagents, whereas the second (Y162-Y163-R164) is labeled at low levels.

The thermal stabilities of untreated PrP^C and the products of its reaction with either 100× PN or 1000× TNM were measured by CD spectroscopy (Figure 7). The temperature at which 50% of untreated PrP^C is unfolded (T_m) was found to be 67 °C. This is higher than the T_m of 61.3 °C reported for the full length protein (*51*), which has a much larger unstructured N-terminal domain than the truncated PrP^C used in this study. Treatment of PrP^C with 1000× TNM did not affect the T_m, whereas the T_m decreased by 9 °C for the 100× PN-treated sample. All samples show some deviation from simple two-state unfolding behavior (*65*), but the effect is more pronounced for the PN-treated sample. Such deviation indicates that localized unfolding occurs in some parts of the protein, and/or that a portion of the total protein in the sample has fully unfolded at temperatures where most of the sample is intact.

Patterns of Tyr Nitration in the β-Oligomer. When PN was used to label the β-oligomer, most Tyr residues that reacted in the PrP^C form were also found to be nitrated, although the reactivity of both Y225 and Y226 substantially decreased (Table 2). The level of mononitration detected in peptide P3 (*157−164*) was similar in both PrP^C and the β-oligomer, and similar patterns of labeling were noted (no labeling at Y157, some labeling at Y163, majority of nitration at Y162). Two additional Tyr (Y149 and Y150) that are inert to nitration by PN in PrP^C are quite reactive in the β-oligomeric conformer. Tandem mass spectrometry showed that both of these residues, which are part of the first YYR motif, are capable of being nitrated, although nitro-Y149 was the dominant product detected. Identical nitration results were obtained for a sample of 250× PN-treated β-oligomer that had been separated from the cross-linked aggregates using the AF_4 methodology.

In stark contrast with the results obtained with PrP^C, TNM was an effective reagent for labeling the β-oligomer even at 100× concentration, and produced a similar pattern of nitro-Tyr formation as 100× PN. The only exception is Y128, which is labeled at low levels by PN in both PrP^C and β-oligomeric conformers but does not react with TNM in either conformation.

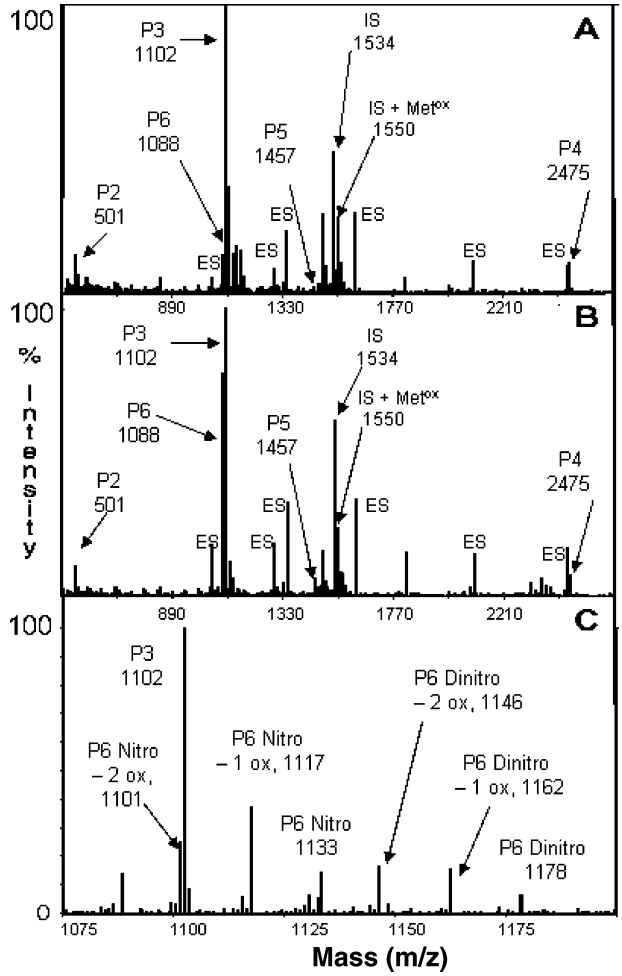

FIGURE 4: A partial MALDI-TOF spectrum of peptides from the tryptic digest of (A) PrP^C and (B) the β-oligomer, after reaction with 100× PN. (C) A closeup of the 1100 *m/z* region of spectrum (A), showing the dinitrated peptides for P6 and the loss of 1 or more oxygen atoms from the nitro group for mono- and dinitrated P6 peptides. ES: External peptide standards of masses 1046, 1296, 1347, 1619, 2093, and 2046. IS: Internal standard (PrP90 tryptic peptide containing residues 137−148).

y ion #	sequence	nitro-Y157	nitro-Y162	nitro-Y163
8	Y_{157}PNQV$Y_{162}Y_{163}$R	1147.53	1147.53	1147.53
7	PNQV$Y_{162}Y_{163}$R	939.49	984.49	984.49
6	NQV$Y_{162}Y_{163}$R	842.41	887.41	887.41
5	QV$Y_{162}Y_{163}$R	728.37	773.37	773.37
4	V$Y_{162}Y_{163}$R	600.31	645.31	645.31
3	$Y_{162}Y_{163}$R	**501.25**	**546.25**	**546.25**
2	Y_{163}R	**338.18**	**338.18**	**383.18**
1	R	175.11	175.11	175.11

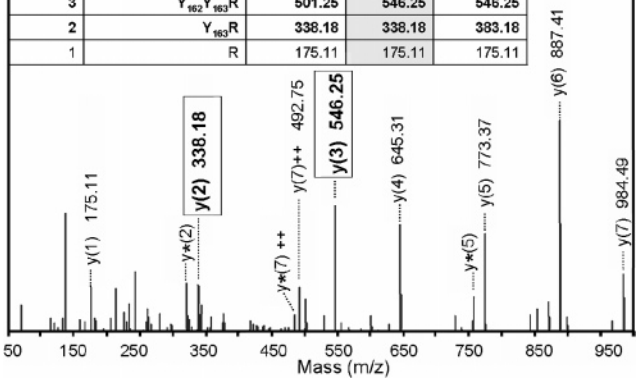

FIGURE 5: ESI-MS/MS spectrum of one mononitrated P3 peptide from the 100× PN/β-oligomer sample. Inset: The masses of the M + H y ions expected from each of the three potential sites of mononitration. (*) The loss of ammonia (−17) from R or Q; (++) doubly charged ions.

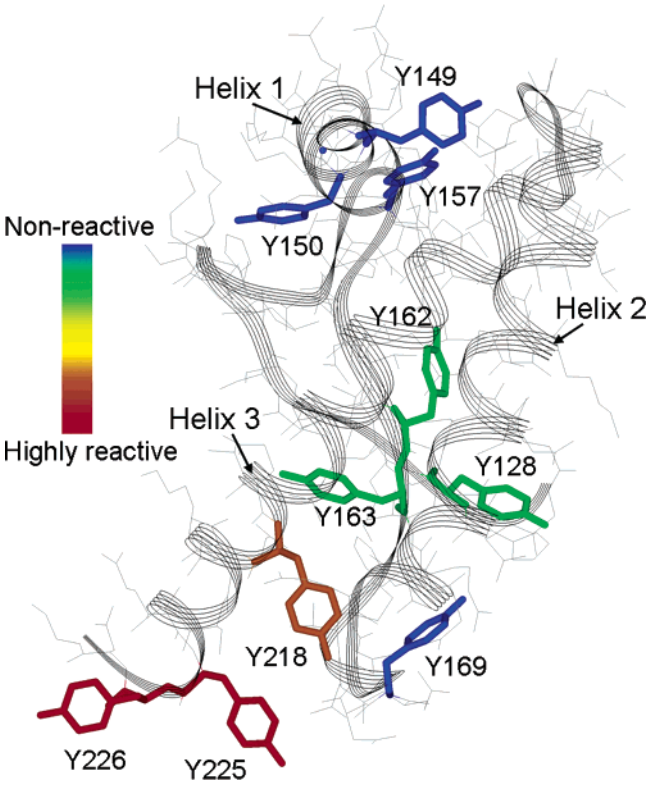

FIGURE 6: Structure of hamster PrP^C (from ref *14*) indicating the locations and relative reactivities of the 10 Tyr residues after treatment with 100× PN.

DISCUSSION

Two nitrating reagents were used to probe for structural differences between PrP^C, the normal cellular form of prion protein, and the β-oligomeric conformer, whose secondary structure is similar to the disease-associated conformation of PrP (*34*, *46*, *66*, *67*). Peroxynitrite (PN) is a water-soluble, powerful oxidant that uses a radical-based reaction mechanism to oxidize several amino acids, including Met, Cys (thiol form), Trp, and Tyr. In addition to the Tyr nitration discussed in this paper, some Met oxidation was also detected when PrP was treated with PN, but neither of the two Trp residues present in residues 90−232 of PrP was modified by PN (data not shown). The reactive form of PN is actually its protonated state, $HONO_2$, (pK_a 6.8) (*68*, *69*), which can oxidize amino acids directly in a bimolecular reaction, but has a half-life of only ∼1 s (*56*). $HONO_2$ decomposes to yield two radical species, hydroxide $OH^\bullet$ and nitrogen dioxide $NO_2^\bullet$. An intermediate reaction with CO_2 produces the carbonate radical $CO_3^{\bullet-}$ and $NO_2^\bullet$ (*69*). Any of these intermediate radicals are capable of oxidizing a Tyr residue to its radical state ($Tyr^\bullet$), which leads to the production of either nitro-Tyr or diTyr cross-links.

The relative reactivity of a Tyr residue with PN is governed by its local protein environment (*70*). In approximate order of importance, these environmental factors that increase reactivity are (i) the lack of reactive Cys residues near the Tyr, (ii) the presence of a negatively charged residue, (iii) the absence of steric hindrance, (iv) surface (solvent) exposure, and (v) the presence of Tyr in a

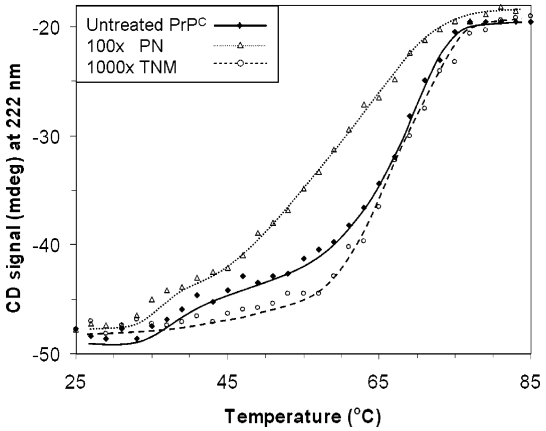

FIGURE 7: Thermal denaturation of PrP^c before and after treatment with 100× PN or 1000× TNM, as followed by the loss in CD signal at 222 nm (loss of α-helicity). (■) Untreated PrP^c control; (Δ) 100× PN reaction; (○) 1000× TNM reaction.

loop secondary structure. Of these, only (i) can be completely ruled out as influencing Tyr reactivity in PrP, since the only two Cys residues present in PrP are involved in disulfide bond formation in both isoforms studied here. However, for PrP^C, which has a well-defined structure, the two Tyr residues that are highly accessible to solvent were labeled with extremely high efficiency.

Tetranitromethane is soluble in organic solvents, and so it is thought to more readily react with buried Tyr residues than PN. However, TNM also readily nitrates surface Tyr residues (*71*). To a lesser extent, its reactivity with Tyr residues is also governed by the protein microenvironment, which includes factors such as steric hindrance, hydrogen bonding to the Tyr hydroxyl group, and the presence of charged residues near the Tyr. It is proposed that Tyr residues with lower pK_a values will be more reactive toward TNM, since the nitration mechanism involves formation of a tyrosinate/TNM charge-transfer complex (*64*). In this regard, the low pH used in this study may limit reactivity with TNM. Interestingly, the most highly buried Tyr residues were unreactive with TNM, while the most solvent exposed Tyr residues were the most reactive. This indicates that solvent exposure is the dominating factor in determining the reactivity of Tyr residues in PrP, for both PN and TNM.

The observed patterns of Tyr nitration for PrP^C (Table 2) support the premise that when the surface exposure of the Tyr residue is not high, its reactivity is influenced by multiple factors. The most readily nitrated Tyr residues (Y225, Y226) are clearly the most highly surface exposed residues. However, non-surface residues are also labeled to some degree. For these, no correlation with the presence of charged amino acids or hydrogen bonding was found. In fact, none of the identified factors that favor nitration are associated with Y218, yet this residue is quite susceptible to nitration in PrP^C. On the whole, the PrP^C data indicate that nitration should not be used to predict *global* protein structure, although it serves as a good indicator of changes in local chemical environment. These changes may be due to backbone or side chain movements, or to the presence of another subunit in the oligomeric state, or both.

PrP^C was surprisingly stable toward TNM treatment. To achieve similar levels of nitration of PrP^C with TNM compared with 100× PN, a 1000-fold excess of reagent (100× over Tyr) was required. Interestingly, the 1000× TNM-labeled PrP^C did not form any cross-linked products (Figure 3) as was noted for PN treatment. Moreover, the thermal denaturation profile (Figure 7), which is a measure of protein stability, was not modified for PrP^C treated with 1000× TNM compared with untreated PrP^C. In contrast, PN treatment of PrP^C destabilized the protein somewhat, as indicated by both the decrease in T_m and the rather large deviation from two-state unfolding behavior. This indicates that either there is some localized unfolding within the PN-treated sample or some population of the PN-treated PrP^C is completely unfolded at lower temperature (is less stable) than the majority of the sample. Since these changes occur only for the 100× PN-treated sample and not for the 1000× TNM-treated sample, they cannot be attributed to the generic heterogeneity associated with a sample composed of partially nitrated proteins. Rather, the destabilization of PrP^C by PN treatment is best explained by modifications of PrP^C that occur only when PN is used as the nitrating reagent. Of the ten Tyr residues, only Y128 is nitrated by PN but not by TNM.

It is quite plausible that the nitration of Tyr128 would lead to protein instability. Tyr128 is adjacent to Met129 and is hydrogen bonded to Asp178 in many of the hamster PrP^C solution structures (*72*). Both Met129 and Asp178 are residues linked to human disease (*73*−*77*). The D178N mutation causes fatal familial insomnia if residue 129 is Met, and causes Creutzfeldt−Jakob disease if the variant Val129 is present. Moreover, the D178N mutation is predicted to eliminate the hydrogen bond between D178 and Y128, leading to the overall destabilization of the protein (*78*, *79*). Thus, the protein destabilization noted in the thermal denaturation might be due to the presence of some nitro-Y128 protein in the ensemble of PN-treated PrP^C proteins. Increasing the PN concentration above 100× was associated with higher levels of nitro-Y128 formation (data not shown) and correlated with higher levels of protein unfolding and cross-linking (Figure 2). Alternatively, the difference in protein stability between PrP^C treated with PN vs TNM may arise from other oxidation events. We have noted that higher levels of Met oxidation occur when PN is the nitrating agent, and cannot rule out that oxidation of Met residues, in particular Met129, influences the overall protein stability, or that Met oxidation leads to the labeling of Y128.

For the β-oligomer, 100× TNM produced the same level of nitration as with 100× PN. The facility with which TNM labeled the β-oligomer was surprising, since PrP^C was relatively inert toward labeling with TNM. (For PrP^C, 1000× TNM was required to achieve levels of nitration similar to those observed with 100× PN.) Evidently formation of the β-oligomer does not prevent either reagent—the hydrophobic TNM or the water soluble PN—from accessing the susceptible Tyr residues. Table 2 shows that the differences in the nitration patterns are clearly isoform-specific but not reagent-specific, with the exception of Y128, which displayed low levels of reactivity to PN (but not TNM) in both isoforms. Interestingly, the two Tyr residues of the C-terminal YYD motif, Y225 and Y226, are ~50% less reactive toward both reagents in the β-oligomer. This was surprising, since none of the published models for fibrillar PrP^{Sc} predict changes in secondary structure occurring in this part of the C-terminal helix. However, the β-spiral model by Demarco and Daggett

(*35*) shows that these residues lie on a helix that is near the subunit interface. It is possible that subunit packing in the β-oligomer, rather than a change in secondary structure, has decreased the solvent accessibility of Y225 and Y226.

For both TNM and PN, the major difference in Tyr nitration between the two PrP isoforms occurs at Y149 and Y150. Y149 was labeled reasonably well and Y150 to a lesser degree by either PN or TNM in the β-oligomeric state, but neither residue was nitrated in the PrP^C isoform. Y149 and Y150 are part of the first conserved YYR motif. Thus, our evidence strongly suggests that the first YYR motif, located on helix 1 of PrP^c, undergoes a significant conformational change upon conversion to the β-oligomer. The data are consistent with these Tyr residues becoming more surface exposed in the β-oligomeric state, although other changes in the microenvironment might also influence the reactivity (*70*). The β-helix model (*32*) for PrP^{Sc} places both Y149 and Y150 in a surface exposed, solvent accessible environment, whereas in the β-spiral model (*35*), only Y149 undergoes a shift in surface exposure. Monoclonal antibody (MAb) work (*40*−*42*) supports the hypothesis that at least one of the YYR motifs becomes more surface accessible in PrP^{Sc}. In one study, anti-YYR antibodies were found to specifically recognize the diseased PrP^{Sc} conformation, which shares similar secondary structure characteristics with the β-oligomer (*40*). However, these authors favor the second YYR motif as being the conformationally sensitive epitope. Other work using the PrP^{Sc}-specific MAb 15B3 (*41*) has identified a sequence containing the second YYR motif as part of its large, discontinuous epitope, but this MAb reportedly also recognizes the sequence immediately preceding the first YYR motif, so the results are not conclusive. A recent publication by Novitskaya et al. (*42*) indicates that antibody AH6 (epitope 159−174) binds to recombinant mouse PrP fibrils only after they are completely denatured by 6 M guanidine-HCl. In contrast, antibody D18 (epitope 132−158) and IgG 136−158 are capable of binding under conditions where the fibrillar structure is still preserved, although neither bound in the absence of guanidine-HCl. Limited experiments were also conducted with the mouse β-oligomer, which also reacted with IgG 136−158 (D18 and AH6 were not tested).

The Tyr nitration results presented here provide an independent and complementary technique to antibody studies. The data clearly show that only the first YYR motif containing Y149 and Y150 is differentially nitrated by the two nitrating reagents PN and TNM. In contrast, the second YYR motif (Y162-Y163-R164) was nitrated only at low levels and in both conformers. This provides very strong evidence that, upon conversion of PrP^C to the β-oligomer, the helix 1 region containing the first YYR motif, residues 149−151, undergoes a large structural change. Alternatively, it is possible that the β-oligomer and PrP^{Sc} are structurally different near the YYR motifs. However, the two structures would have to be precisely and reciprocally different, with only the first YYR exposed in the β-oligomer and only the second YYR exposed in PrP^{Sc}. Thus, we favor assignment of the first YYR as the antigenic site. Another change in the local chemical environment was noted for Y225 and Y226 of helix 3. These residues showed a substantial decrease in nitration susceptibility in the β-oligomer. The global similarities between the β-oligomer and the physiologically relevant PrP^{Sc} isoform suggest that the conformational changes noted for the β-oligomer may have biological significance. Future experiments will examine the interactions of various MAbs with the nitrated PrP samples, and extend the nitration studies to include the recombinant fibrillar PrP and the PrP^{Sc} isoforms.

ACKNOWLEDGMENT

We thank Dr. Valerie Daggett and Dr. Cedric Govaerts for providing us with the PDB coordinates for their models, and Ms. Martha Rice for technical assistance.

REFERENCES

1. Priola, S. A., Chesebro, B., and Caughey, B. (2003) Biomedicine. A view from the top—prion diseases from 10,000 feet, *Science 300*, 917−9.
2. Prusiner, S. B. (1998) Prions, *Proc. Natl. Acad. Sci. U.S.A. 95*, 13363−83.
3. Tan, S. Y., and Pepys, M. B. (1994) Amyloidosis, *Histopathology 25*, 403−14.
4. Caughey, B., Raymond, G. J., Callahan, M. A., Wong, C., Baron, G. S., and Xiong, L. W. (2001) Interactions and conversions of prion protein isoforms, *Adv. Protein Chem. 57*, 139−69.
5. Prusiner, S. B. (1982) Novel proteinaceous infectious particles cause scrapie, *Science 216*, 136−44.
6. Caughey, B. W., Dong, A., Bhat, K. S., Ernst, D., Hayes, S. F., and Caughey, W. S. (1991) Secondary structure analysis of the scrapie-associated protein PrP 27-30. in water by infrared spectroscopy, *Biochemistry 30*, 7672−80.
7. Stahl, N., Baldwin, M. A., Teplow, D. B., Hood, L., Gibson, B. W., Burlingame, A. L., and Prusiner, S. B. (1993) Structural studies of the scrapie prion protein using mass spectrometry and amino acid sequencing, *Biochemistry 32*, 1991−2002.
8. Zahn, R., Liu, A., Luhrs, T., Riek, R., von Schroetter, C., Lopez Garcia, F., Billeter, M., Calzolai, L., Wider, G., and Wuthrich, K. (2000) NMR solution structure of the human prion protein, *Proc. Natl. Acad. Sci. U.S.A. 97*, 145−50.
9. Zahn, R., Guntert, P., von Schroetter, C., and Wuthrich, K. (2003) NMR structure of a variant human prion protein with two disulfide bridges, *J. Mol. Biol. 326*, 225−34.
10. Riek, R., Hornemann, S., Wider, G., Billeter, M., Glockshuber, R., and Wuthrich, K. (1996) NMR structure of the mouse prion protein domain PrP(121-321), *Nature 382*, 180−2.
11. Lysek, D. A., Schorn, C., Nivon, L. G., Esteve-Moya, V., Christen, B., Calzolai, L., von Schroetter, C., Fiorito, F., Herrmann, T., Guntert, P., and Wuthrich, K. (2005) Prion protein NMR structures of cats, dogs, pigs, and sheep, *Proc. Natl. Acad. Sci. U.S.A. 102*, 640−5.
12. Lopez Garcia, F., Zahn, R., Riek, R., and Wuthrich, K. (2000) NMR structure of the bovine prion protein, *Proc. Natl. Acad. Sci. U.S.A. 97*, 8334−9.
13. Calzolai, L., Lysek, D. A., Perez, D. R., Guntert, P., and Wuthrich, K. (2005) Prion protein NMR structures of chickens, turtles, and frogs, *Proc. Natl. Acad. Sci. U.S.A. 102*, 651−5.
14. James, T. L., Liu, H., Ulyanov, N. B., Farr-Jones, S., Zhang, H., Donne, D. G., Kaneko, K., Groth, D., Mehlhorn, I., Prusiner, S. B., and Cohen, F. E. (1997) Solution structure of a 142-residue recombinant prion protein corresponding to the infectious fragment of the scrapie isoform, *Proc. Natl. Acad. Sci. U.S.A. 94*, 10086−91.
15. Gossert, A. D., Bonjour, S., Lysek, D. A., Fiorito, F., and Wuthrich, K. (2005) Prion protein NMR structures of elk and of mouse/elk hybrids, *Proc. Natl. Acad. Sci. U.S.A. 102*, 646−50.
16. Haire, L. F., Whyte, S. M., Vasisht, N., Gill, A. C., Verma, C., Dodson, E. J., Dodson, G. G., and Bayley, P. M. (2004) The crystal structure of the globular domain of sheep prion protein, *J. Mol. Biol. 336*, 1175−83.
17. Knaus, K. J., Morillas, M., Swietnicki, W., Malone, M., Surewicz, W. K., and Yee, V. C. (2001) Crystal structure of the human prion protein reveals a mechanism for oligomerization, *Nat. Struct. Biol. 8*, 770−4.
18. Eghiaian, F., Grosclaude, J., Lesceu, S., Debey, P., Doublet, B., Treguer, E., Rezaei, H., and Knossow, M. (2004) Insight into the PrPC→PrPSc conversion from the structures of antibody-bound

ovine prion scrapie-susceptibility variants, *Proc. Natl. Acad. Sci. U.S.A. 101*, 10254−9.
19. Wuthrich, K., and Riek, R. (2001) Three-dimensional structures of prion proteins, *Adv. Protein Chem. 57*, 55−82.
20. Merz, P. A., Kascsak, R. J., Rubenstein, R., Carp, R. I., and Wisniewski, H. M. (1987) Antisera to scrapie-associated fibril protein and prion protein decorate scrapie-associated fibrils, *J. Virol. 61*, 42−9.
21. Prusiner, S. B., McKinley, M. P., Bowman, K. A., Bolton, D. C., Bendheim, P. E., Groth, D. F., and Glenner, G. G. (1983) Scrapie prions aggregate to form amyloid-like birefringent rods, *Cell 35*, 349−58.
22. Caughey, B. (2001) Interactions between prion protein isoforms: the kiss of death?, *Trends Biochem. Sci. 26*, 235−42.
23. Baskakov, I. V., Aagaard, C., Mehlhorn, I., Wille, H., Groth, D., Baldwin, M. A., Prusiner, S. B., and Cohen, F. E. (2000) Self-assembly of recombinant prion protein of 106 residues, *Biochemistry 39*, 2792−804.
24. Flechsig, E., Shmerling, D., Hegyi, I., Raeber, A. J., Fischer, M., Cozzio, A., von Mering, C., Aguzzi, A., and Weissmann, C. (2000) Prion protein devoid of the octapeptide repeat region restores susceptibility to scrapie in PrP knockout mice, *Neuron 27*, 399−408.
25. Supattapone, S., Muramoto, T., Legname, G., Mehlhorn, I., Cohen, F. E., DeArmond, S. J., Prusiner, S. B., and Scott, M. R. (2001) Identification of two prion protein regions that modify scrapie incubation time, *J. Virol. 75*, 1408−13.
26. Fischer, M., Rulicke, T., Raeber, A., Sailer, A., Moser, M., Oesch, B., Brandner, S., Aguzzi, A., and Weissmann, C. (1996) Prion protein (PrP) with amino-proximal deletions restoring susceptibility of PrP knockout mice to scrapie, *EMBO J. 15*, 1255−64.
27. Frankenfield, K. N., Powers, E. T., and Kelly, J. W. (2005) Influence of the N-terminal domain on the aggregation properties of the prion protein, *Protein Sci. 14*, 2154−66.
28. Lawson, V. A., Priola, S. A., Wehrly, K., and Chesebro, B. (2001) N-terminal truncation of prion protein affects both formation and conformation of abnormal protease-resistant prion protein generated in vitro, *J. Biol. Chem. 276*, 35265−71.
29. Lawson, V. A., Priola, S. A., Meade-White, K., Lawson, M., and Chesebro, B. (2004) Flexible N-terminal region of prion protein influences conformation of protease-resistant prion protein isoforms associated with cross-species scrapie infection in vivo and in vitro, *J. Biol. Chem. 279*, 13689−95.
30. Pan, K. M., Baldwin, M., Nguyen, J., Gasset, M., Serban, A., Groth, D., Mehlhorn, I., Huang, Z., Fletterick, R. J., Cohen, F. E., and Prusiner, S. B. (1993) Conversion of alpha-helices into beta-sheets features in the formation of the scrapie prion proteins, *Proc. Natl. Acad. Sci. U.S.A. 90*, 10962−6.
31. Wille, H., Michelitsch, M. D., Guenebaut, V., Supattapone, S., Serban, A., Cohen, F. E., Agard, D. A., and Prusiner, S. B. (2002) Structural studies of the scrapie prion protein by electron crystallography, *Proc. Natl. Acad. Sci. U.S.A. 99*, 3563−8.
32. Govaerts, C., Wille, H., Prusiner, S. B., and Cohen, F. E. (2004) Evidence for assembly of prions with left-handed beta-helices into trimers, *Proc. Natl. Acad. Sci. U.S.A. 101*, 8342−7.
33. Anderson, M., Bocharova, O. V., Makarava, N., Breydo, L., Salnikov, V. V., and Baskakov, I. V. (2006) Polymorphism and ultrastructural organization of prion protein amyloid fibrils: an insight from high resolution atomic force microscopy, *J. Mol. Biol. 358*, 580−96.
34. Tattum, M. H., Cohen-Krausz, S., Khalili-Shirazi, A., Jackson, G. S., Orlova, E. V., Collinge, J., Clarke, A. R., and Saibil, H. R. (2006) Elongated oligomers assemble into mammalian PrP amyloid fibrils, *J. Mol. Biol. 357*, 975−85.
35. DeMarco, M. L., and Daggett, V. (2004) From conversion to aggregation: protofibril formation of the prion protein, *Proc. Natl. Acad. Sci. U.S.A. 101*, 2293−8.
36. Malolepsza, E., Boniecki, M., Kolinski, A., and Piela, L. (2005) Theoretical model of prion propagation: a misfolded protein induces misfolding, *Proc. Natl. Acad. Sci. U.S.A. 102*, 7835−40.
37. Langedijk, J. P., Fuentes, G., Boshuizen, R., and Bonvin, A. M. (2006) Two-rung model of a left-handed beta-helix for prions explains species barrier and strain variation in transmissible spongiform encephalopathies, *J. Mol. Biol. 360*, 907−920.
38. Yang, S., Levine, H., Onuchic, J. N., and Cox, D. L. (2005) Structure of infectious prions: stabilization by domain swapping, *FASEB J. 19*, 1778−82.
39. Cox, D. L., Pan, J., and Singh, R. R. (2006) A mechanism for copper inhibition of infectious prion conversion, *Biophys. J. 91*, L11−3.
40. Paramithiotis, E., Pinard, M., Lawton, T., LaBoissiere, S., Leathers, V. L., Zou, W. Q., Estey, L. A., Lamontagne, J., Lehto, M. T., Kondejewski, L. H., Francoeur, G. P., Papadopoulos, M., Haghighat, A., Spatz, S. J., Head, M., Will, R., Ironside, J., O'Rourke, K., Tonelli, Q., Ledebur, H. C., Chakrabartty, A., and Cashman, N. R. (2003) A prion protein epitope selective for the pathologically misfolded conformation, *Nat. Med. 9*, 893−9.
41. Korth, C., Stierli, B., Streit, P., Moser, M., Schaller, O., Fischer, R., Schulz-Schaeffer, W., Kretzschmar, H., Raeber, A., Braun, U., Ehrensperger, F., Hornemann, S., Glockshuber, R., Riek, R., Billeter, M., Wuthrich, K., and Oesch, B. (1997) Prion (PrPSc)-specific epitope defined by a monoclonal antibody, *Nature 390*, 74−7.
42. Novitskaya, V., Makarava, N., Bellon, A., Bocharova, O. V., Bronstein, I. B., Williamson, R. A., and Baskakov, I. V. (2006) Probing the conformation of the prion protein within a single amyloid fibril using a novel immunoconformational assay, *J. Biol. Chem. 281*, 15536−45.
43. Moroncini, G., Mangieri, M., Morbin, M., Mazzoleni, G., Ghetti, B., Gabrielli, A., Williamson, R. A., Giaccone, G., and Tagliavini, F. (2006) Pathologic prion protein is specifically recognized in situ by a novel PrP conformational antibody, *Neurobiol. Dis. 23*, 717−24.
44. Bocharova, O. V., Breydo, L., Parfenov, A. S., Salnikov, V. V., and Baskakov, I. V. (2005) In vitro conversion of full-length mammalian prion protein produces amyloid form with physical properties of PrP(Sc), *J. Mol. Biol. 346*, 645−59.
45. Legname, G., Baskakov, I. V., Nguyen, H. O., Riesner, D., Cohen, F. E., DeArmond, S. J., and Prusiner, S. B. (2004) Synthetic mammalian prions, *Science 305*, 673−6.
46. Baskakov, I. V., Legname, G., Baldwin, M. A., Prusiner, S. B., and Cohen, F. E. (2002) Pathway complexity of prion protein assembly into amyloid, *J. Biol. Chem. 277*, 21140−8.
47. Vendrely, C., Valadie, H., Bednarova, L., Cardin, L., Pasdeloup, M., Cappadoro, J., Bednar, J., Rinaudo, M., and Jamin, M. (2005) Assembly of the full-length recombinant mouse prion protein I. Formation of soluble oligomers, *Biochim. Biophys. Acta 1724*, 355−66.
48. Silveira, J. R., Raymond, G. J., Hughson, A. G., Race, R. E., Sim, V. L., Hayes, S. F., and Caughey, B. (2005) The most infectious prion protein particles, *Nature 437*, 257−61.
49. Turko, I. V., and Murad, F. (2005) Mapping sites of tyrosine nitration by matrix-assisted laser desorption/ionization mass spectrometry, *Methods Enzymol. 396*, 266−75.
50. Wong, P. S., and van der Vliet, A. (2002) Quantitation and localization of tyrosine nitration in proteins, *Methods Enzymol. 359*, 399−410.
51. Speare, J. O., Rush, T. S., 3rd, Bloom, M. E., and Caughey, B. (2003) The role of helix 1 aspartates and salt bridges in the stability and conversion of prion protein, *J. Biol. Chem. 278*, 12522−9.
52. Sambrook, J., and Russell, D. W. (2001) *Molecular Cloning, A Laboratory Manual*, 3rd ed., Cold Spring Harbor Laboratory Press, New York.
53. Baskakov, I. V., Legname, G., Prusiner, S. B., and Cohen, F. E. (2001) Folding of prion protein to its native alpha-helical conformation is under kinetic control, *J. Biol. Chem. 276*, 19687−90.
54. Pace, C. N., Vajdos, F., Fee, L., Grimsley, G., and Gray, T. (1995) How to measure and predict the molar absorption coefficient of a protein, *Protein Sci. 11*, 2411−2423.
55. King, P. A., Jamison, E., Strahs, D., Anderson, V. E., and Brenowitz, M. (1993) 'Footprinting' proteins on DNA with peroxonitrous acid, *Nucleic Acids Res. 21*, 2473−8.
56. Sarver, A., Scheffler, N. K., Shetlar, M. D., and Gibson, B. W. (2001) Analysis of peptides and proteins containing nitrotyrosine by matrix-assisted laser desorption/ionization mass spectrometry, *J. Am. Soc. Mass Spectrom. 12*, 439−48.
57. Koradi, R., Billeter, M., and Wuthrich, K. (1996) MOLMOL: a program for display and analysis of macromolecular structures, *J. Mol. Graphics 14*, 51−5, 29−32.
58. Lobley, A., Whitmore, L., and Wallace, B. A. (2002) DICHROWEB: an interactive website for the analysis of protein secondary structure from circular dichroism spectra, *Bioinformatics 18*, 211−2.

59. Whitmore, L., and Wallace, B. A. (2004) DICHROWEB, an online server for protein secondary structure analyses from circular dichroism spectroscopic data, *Nucleic Acids Res. 32*, W668−73.
60. Sokolowski, F., Modler, A. J., Masuch, R., Zirwer, D., Baier, M., Lutsch, G., Moss, D. A., Gast, K., and Naumann, D. (2003) Formation of critical oligomers is a key event during conformational transition of recombinant Syrian hamster prion protein, *J. Biol. Chem. 278*, 40481−92.
61. Rezaei, H., Eghiaian, F., Perez, J., Doublet, B., Choiset, Y., Haertle, T., and Grosclaude, J. (2005) Sequential generation of two structurally distinct ovine prion protein soluble oligomers displaying different biochemical reactivities, *J. Mol. Biol. 347*, 665−79.
62. Hirel, P. H., Schmitter, M. J., Dessen, P., Fayat, G., and Blanquet, S. (1989) Extent of N-terminal methionine excision from *Escherichia coli* proteins is governed by the side-chain length of the penultimate amino acid, *Proc. Natl. Acad. Sci. U.S.A. 86*, 8247−51.
63. Lee, T. D., and Shively, J. E. (1990) Enzymatic and chemical digestion of proteins for mass spectrometry, *Methods Enzymol. 193*, 361−74.
64. Bruice, T. C., Gregory, M. J., and Walters, S. L. (1968) Reactions of tetranitromethane. I. Kinetics and mechanism of nitration of phenols by tetranitromethane, *J. Am. Chem. Soc. 90*, 1612.
65. Eftink, M. R. (1995) Use of multiple spectroscopic methods to monitor equilibrium unfolding of proteins, *Methods Enzymol. 259*, 487−512.
66. Leffers, K. W., Wille, H., Stohr, J., Junger, E., Prusiner, S. B., and Riesner, D. (2005) Assembly of natural and recombinant prion protein into fibrils, *Biol. Chem. 386*, 569−80.
67. Novitskaya, V., Bocharova, O. V., Bronstein, I., and Baskakov, I. V. (2006) Amyloid fibrils of mammalian prion protein are highly toxic to cultured cells and primary neurons, *J. Biol. Chem. 281*, 13828−36.
68. Batthyany, C., Souza, J. M., Duran, R., Cassina, A., Cervenansky, C., and Radi, R. (2005) Time course and site (s) of cytochrome c tyrosine nitration by peroxynitrite, *Biochemistry 44*, 8038−46.
69. Radi, R., Cassina, A., Hodara, R., Quijano, C., and Castro, L. (2002) Peroxynitrite reactions and formation in mitochondria, *Free Radical Biol. Med. 33*, 1451−64.
70. Souza, J. M., Daikhin, E., Yudkoff, M., Raman, C. S., and Ischiropoulos, H. (1999) Factors determining the selectivity of protein tyrosine nitration, *Arch. Biochem. Biophys. 371*, 169−78.
71. Petersson, A. S., Steen, H., Kalume, D. E., Caidahl, K., and Roepstorff, P. (2001) Investigation of tyrosine nitration in proteins by mass spectrometry, *J. Mass Spectrom. 36*, 616−25.
72. Liu, H., Farr-Jones, S., Ulyanov, N. B., Llinas, M., Marqusee, S., Groth, D., Cohen, F. E., Prusiner, S. B., and James, T. L. (1999) Solution structure of Syrian hamster prion protein rPrP(90−231), *Biochemistry 38*, 5362−77.
73. Apetri, A. C., Vanik, D. L., and Surewicz, W. K. (2005) Polymorphism at residue 129 modulates the conformational conversion of the D178N variant of human prion protein 90−231, *Biochemistry 44*, 15880−8.
74. Baskakov, I., Disterer, P., Breydo, L., Shaw, M., Gill, A., James, W., and Tahiri-Alaoui, A. (2005) The presence of valine at residue 129 in human prion protein accelerates amyloid formation, *FEBS Lett. 579*, 2589−96.
75. Gambetti, P. (1996) Fatal familial insomnia and familial Creutzfeldt-Jakob disease: a tale of two diseases with the same genetic mutation, *Curr. Top. Microbiol. Immunol. 207*, 19−25.
76. Zarranz, J. J., Digon, A., Atares, B., Rodriguez-Martinez, A. B., Arce, A., Carrera, N., Fernandez-Manchola, I., Fernandez-Martinez, M., Fernandez-Maiztegui, C., Forcadas, I., Galdos, L., Gomez-Esteban, J. C., Ibanez, A., Lezcano, E., Lopez de Munain, A., Marti-Masso, J. F., Mendibe, M. M., Urtasun, M., Uterga, J. M., Saracibar, N., Velasco, F., and de Pancorbo, M. M. (2005) Phenotypic variability in familial prion diseases due to the D178N mutation, *J. Neurol. Neurosurg. Psychiatry 76*, 1491−6.
77. Gambetti, P., Parchi, P., and Chen, S. G. (2003) Hereditary Creutzfeldt-Jakob disease and fatal familial insomnia, *Clin. Lab. Med. 23*, 43−64.
78. Barducci, A., Chelli, R., Procacci, P., Schettino, V., Gervasio, F. L., and Parrinello, M. (2006) Metadynamics simulation of prion protein: beta-structure stability and the early stages of misfolding, *J. Am. Chem. Soc. 128*, 2705−10.
79. Gsponer, J., Ferrara, P., and Caflisch, A. (2001) Flexibility of the murine prion protein and its Asp178Asn mutant investigated by molecular dynamics simulations, *J. Mol. Graphics Modell. 20*, 169−82.

BI0617254